remote sensing

MDPI

Article

Intensified and Extended Growing Seasons in *Abies marocana* Forests (2000–2024): A Robust Seasonal Trend Analysis Using 16-Day MODIS EVI Time Series

Oliver Gutiérrez-Hernández [1,*] and Luis V. García [2]

[1] University of Málaga (UMA), 29071 Málaga, Spain
[2] Institute of Natural Resources and Agrobiology of Seville (IRNAS), Spanish National Research Council (CSIC), 41012 Seville, Spain; lv.garcia@csic.es
* Correspondence: olivergh@uma.es

Highlights

What are the main findings?

- We developed Robust Seasonal Trend Analysis (RSTA), an inferential extension of Seasonal Trend Analysis (STA) that reduces the risk of false positives arising from serial correlation, spatial autocorrelation, and multiple testing in spatiotemporal analyses of seasonal trends.
- We applied RSTA to *Abies marocana* forest cover for the first time, demonstrating that inferential filtering reduced significant trend detections from 86.4% to 79.2% while preserving strong evidence of widespread greening and growing-season extension, and removing marginal browning trends identified by STA.

What are the implications of the main findings?

- RSTA provides a robust framework for analysing seasonal trends in land surface phenology, balancing statistical power and false-positive control while reducing spurious trend detection in spatiotemporal analyses.
- Under ongoing climate warming, the observed extension and intensification of vegetation activity may increase ecosystem water demand, potentially exacerbating drought stress and wildfire vulnerability in Mediterranean forest ecosystems subjected to severe summer drought.

Abstract

We modelled, for the first time, the seasonal dynamics and long-term trends of *Abies marocana* forests (Rif Mountains, northern Morocco) using remote-sensing-derived vegetation indices. Using the MODIS Terra Vegetation Indices product MOD13Q1 (enhanced vegetation index, EVI; 16-day frequency; 250 m spatial resolution) from 2000 to 2024 (575 images over 25 years), we applied a robust seasonal trend analysis (RSTA) workflow, representing an inferential extension of classical seasonal trend analysis (STA) through the explicit control of Type I error under serial and spatial correlation. This approach combined: (i) harmonic regression to capture the annual and semi-annual cycles of *A. marocana* forests, estimating seasonal amplitudes and phases while filtering out low-frequency noise; (ii) an iterative trend-free prewhitening (TFPW) procedure following Wang and Swail, applied only to time series with significant serial autocorrelation according to the Durbin–Watson test; (iii) the Theil–Sen slope (TS) estimator, a robust non-parametric method, to quantify the magnitude and direction of seasonality trends; (iv) the contextual Mann–Kendall (CMK) test to assess the statistical significance of seasonality trends, while correcting for spatial

Check for updates

Academic Editor: Eric Casella

Received: 23 February 2026
Revised: 20 May 2026
Accepted: 26 May 2026
Published: 22 June 2026

Copyright: © 2026 by the authors. Licensee MDPI, Basel, Switzerland. This article is an open access article distributed under the terms and conditions of the Creative Commons Attribution (CC BY) license.

autocorrelation and accounting for cross-correlation among neighbouring pixels; (v) the Benjamini–Hochberg (BH) procedure to control the false discovery rate (FDR), ensuring that only statistically robust seasonality trends were retained; and (vi) reconstruction of seasonal curves representing the beginning and end of the study period and derivation of phenological metrics from the statistically significant seasonal trends retained after inferential filtering. After applying the complete analytical workflow, statistically significant trends were detected in 79.2% of pixels within *A. marocana* forests, compared with 86.4% when prewhitening and false discovery rate control were not applied. All Theil–Sen slopes retained by the RSTA workflow were positive, with a mean slope of approximately 0.00175 EVI year^{-1}, corresponding to an average annual increase of roughly 0.7% and an overall increase of approximately 15% over the 2000–2024 study period relative to the initial mean EVI conditions. Browning trends identified by classical STA were not supported after inferential filtering and FDR control, indicating that all these patterns were spurious or only marginal, and confined to limited areas and edge zones. The reconstructed seasonal trend curves were consistent with a longer growing season, although this inference is based on land-surface vegetation dynamics rather than direct phenological observations. The long-term ecological consequences of these changes in seasonal vegetation activity will hinge on the interactions among warming, rising water demand, and potential disturbance regimes under future climatic conditions.

Keywords: *circum-Mediterranean firs*; Baetic-Rifan firs; *Abies marocana*; *Abies pinsapo*; Intercontinental Biosphere Reserve of the Mediterranean; land surface phenology (LSP); seasonal trend analysis (STA); robust trend analysis (RTA); false discovery rate (FDR); greening trends

1. Introduction

1.1. The Moroccan Fir: The South-Westernmost Circum-Mediterranean Fir

Abies marocana Trab. [1], the Moroccan fir [2], is a Tertiary relict conifer of the family Pinaceae [3], endemic to the Rif Mountains of northern Morocco [4], and represents the south-westernmost taxon of the circum-Mediterranean firs (Figure 1). This group is generally characterised by its fragmented relict distribution in isolated mountain ranges, where topography moderates the harshness of the surrounding Mediterranean conditions, as well as by its high vulnerability to climatic and anthropogenic pressures [5,6].

A. marocana is a long-lived Mediterranean fir, reaching up to 40 m, closely related to *A. pinsapo* [7,8]. It forms either pure stands on favourable shaded slopes or mixed forests with other conifers and broad-leaved species [9].

In the Rif Mountains (northern Morocco), it occupies cold, humid montane niches that contrast with the surrounding arid Mediterranean climate [10], as detailed in the Section 2.1 (Study Area). These climatic conditions, shared with other circum-Mediterranean firs [6], define its current distribution and forest formations, and shape its vegetation dynamics and seasonal patterns.

Given its habitat specialisation in humid to perhumid high-mountain environments of the western Rif, typically between 1500 and 2100 m a.s.l., with mean annual temperatures of 12–14 °C and annual precipitation ranging from 600 to over 2000 mm [11,12], *A. marocana* phenology is highly sensitive to climatic shifts [13]. Therefore, analysing its land-surface phenology is critical to understanding the resilience of these relict forests and their responses to ongoing environmental change within a global remote-sensing framework.



Figure 1. Distribution of the circum-Mediterranean Fir Group with *Abies marocana* at the southwesternmost limit (Talassemtane National Park, Morocco; 35.05°N, 5.15°W). Note: *sensu stricto*, the group's southern range limit is represented by the Mount Lebanon occurrence of *Abies cilicica* (Horsh Ehden, Lebanon; 34.18°N, 35.59°W); although *A. cilicica* is otherwise distributed further north in southern Anatolia (Taurus Mountains; Turkey, ≈36–38.5°N), *A. marocana* has the most southerly mean latitudinal position across its overall range (≈35.1°N). The green circle highlights the location of *A. marocana* forests in the Rif Mountains (northern Morocco). Source: Author's work.

1.2. Vegetation Dynamics Under Climate Change: Modelling Seasonality and Trend Detection Using Remote Sensing

In remote sensing, vegetation dynamics refers to the spatiotemporal variation in vegetation spectral properties at the Earth's surface [14]. Seasonality, as a central component of vegetation dynamics, reflects the periodic responses of ecosystems primarily to climatic drivers associated with the annual cycle and seasonal changes [15].

Advances in international observation programmes, which provide abundant open-access satellite data, have made the monitoring of the Earth's surface a central focus of geoscientific research [16]. By design, these programmes ensure consistent and repeatable observations at regular intervals, making remote sensing an ideal tool for trend analysis in ecological and environmental studies [17].

Vegetation seasonality, as captured by satellite-derived indices, provides a proxy for ecosystem phenology by reflecting the timing and intensity of seasonal growth cycles [18]. Land surface phenology (LSP) captures vegetation phenology at different scales using satellite optical observations [19]. In this sense, vegetation indices are essential for studying vegetation dynamics and land surface phenology [20]. They record the timing and intensity of growth cycles, making them indispensable for analysing changes and trends in seasonality [15].

Ongoing climate change is altering abiotic seasonal cycles (e.g., extended summers), with direct consequences for the phenological patterns they regulate [21]. The temperature

in Mediterranean climate-type regions has increased more rapidly than the global mean rates [22]. Consistent with this pattern, long-term climatic analyses in northwestern Rif regions covering the 1970–2019 period have reported significant warming trends, including increases of up to 1.1 °C in minimum temperatures and 2.6 °C in maximum temperatures [23]. The Mediterranean basin, a global biodiversity hotspot [24], provides a natural laboratory for studying ecosystem adaptation in a rapidly changing environment [25]. Mediterranean ecosystems are particularly vulnerable to climate change and the associated increase in climate anomalies and trends [26]. Rising temperatures represent the main threat to the diversity and survival of Mediterranean forests [27]. In this context, the future of Mediterranean mountain forests remains highly uncertain [28]. Characterising their seasonality, phenology, and long-term trends is essential to understanding ecosystem responses and guiding effective conservation strategies.

Remote sensing offers a powerful way to address these challenges within the framework of land surface phenology [29], which enables the detection of ecosystem responses to climatic forcing across broad spatial and temporal scales [30]. To this end, it is crucial to use vegetation indices with reduced saturation [31], such as the enhanced vegetation index (EVI), which more reliably captures seasonal dynamics both in dense canopies—characteristic of fir forests—and in landscapes where the presence of rocky outcrops and open patches can bias spectral responses, compared with the more widely used normalised difference vegetation index (NDVI) [32]. At the same time, detecting long-term trends in seasonality requires robust trend estimators resistant to noise and outliers [33], together with statistical procedures that account for both serial and spatial dependence, since temporal autocorrelation can inflate the significance of monotonic trends over time [34], whereas spatial dependence may artificially increase the apparent extent and coherence of significant patterns across neighbouring pixels [35]. Finally, to ensure that only genuinely significant signals are retained when thousands of pixels are tested simultaneously, it is essential to apply multiple-testing corrections [36–38]. This step is often omitted in remote sensing studies [39]. However, the joint integration of these components—seasonal modelling with non-saturating vegetation indices, robust trend estimation accounting for spatial dependence, and multiple-testing correction in a spatially explicit framework—has not previously been undertaken at the forest cover scale in Mediterranean forest ecosystems.

1.3. Research Gaps and Objectives

The Moroccan fir, the south-westernmost representative of the circum-Mediterranean firs, has often been subsumed under its close relative, the Spanish fir, and has therefore received less specific attention in ecological research and conservation studies [7,12]. This is particularly relevant in Mediterranean mountain ecosystems, where global warming imposes severe constraints on relict high-elevation forests [40–42].

To address this shortcoming, we analysed satellite-derived vegetation indices to model the seasonality of *A. marocana* forests using an extended Seasonal Trend Analysis framework (RSTA), which integrates Seasonal Trend Analysis (STA), an iterative trend-free prewhitening (TFPW) procedure to reduce temporal autocorrelation effects prior to applying a contextual Mann–Kendall (CMK) test, and false discovery rate (FDR) control to account for spatial multiple testing. By explicitly accounting for temporal autocorrelation, spatial context, and multiple testing, the proposed framework improves the statistical robustness and spatial reliability of phenological trend detection in long-term remote sensing time series.

Therefore, our objectives were twofold: (i) to characterise spatiotemporal trends in the seasonality of *A. marocana* forests using a 25-year MODIS EVI time series (2000–2024);

and (ii) to evaluate the effectiveness of the RSTA methodological approach in detecting significant phenological shifts and generating spatially explicit maps of forest dynamics.

Evidence suggests that climate warming has advanced the onset of spring and delayed the arrival of winter, resulting in extended periods of vegetation activity in many temperate and boreal ecosystems of the Northern Hemisphere [43]. Similar phenological shifts are also expected in Mediterranean mountain fir forests and have already been identified in closely related ecosystems such as *A. pinsapo* forests [44]. In this context, we tested the hypothesis that ongoing climate warming is driving significant shifts in the vegetation activity of *A. marocana* forests, resulting in extended growing seasons.

2. Materials and Methods

2.1. Study Area

Talassemtane National Park (~64,000 hectares) is a protected area in the western Rif Mountains of northern Morocco, located in the Tanger–Tetouan–Al Hoceima region, near the historic, cultural, and tourist destination of Chefchaouen (Figure 2).

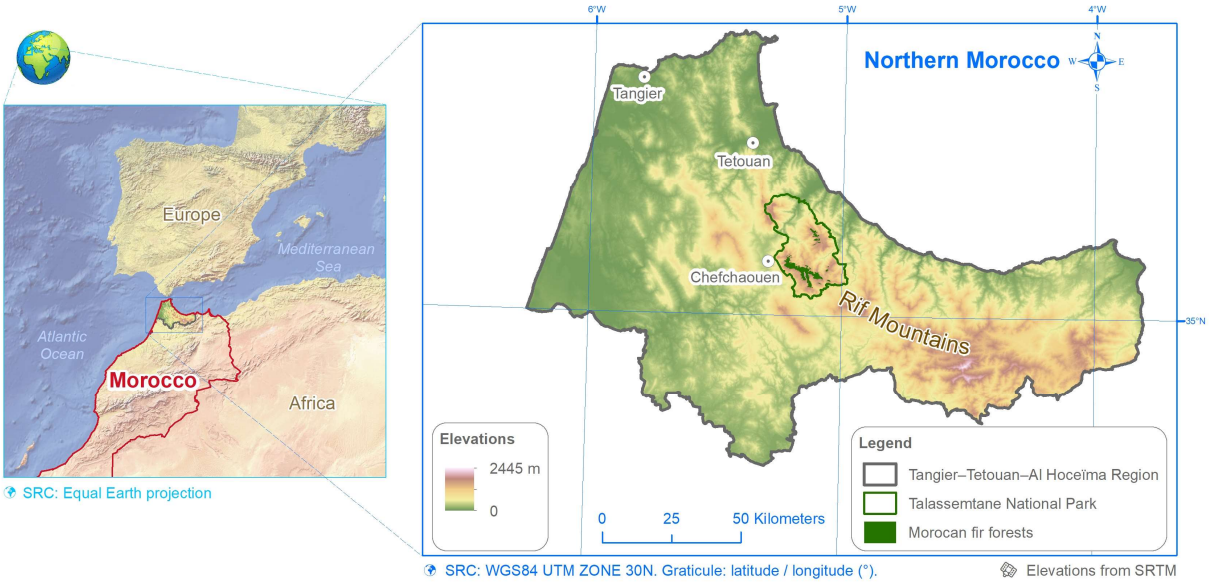


Figure 2. Location and regional context of the Moroccan fir forests in Talassemtane National Park, situated in the western Rif Mountains, northern Morocco. Source: Author's work.

This area includes the distributional range of the Moroccan fir (*Abies marocana* Trab.), which is endemic to the western Rif Mountains and represents the south-westernmost population of the circum-Mediterranean firs. *A. marocana* forests occupy rugged calcareous and dolomitic terrain, with steep slopes and elevations mainly between 1500 and 2100 m a.s.l. [12]. It corresponds to a humid to perhumid montane Mediterranean bioclimatic context, with a pronounced summer drought, and can be classified as Csb according to the Köppen–Geiger climate classification [45]. Within this environmental setting, *A. marocana* forms both pure stands and mixed forest formations, preferentially occupying north-, east-, and west-facing slopes [12,13] (Figure 3). At the community level, *A. marocana* is recurrently associated with *Cedrus atlantica*, *Pinus nigra* subsp. *mauretanica*, *Pinus pinaster* var. maghrebiana, *Quercus rotundifolia*, and *Quercus faginea*, while other woody species such as *Acer opalus* subsp. granatense, *Juniperus oxycedrus*, and *Crataegus laciniata* occur less frequently [9,12,46].



Figure 3. Pure forests and mixed stands dominated by *Abies marocana* in the Rif Mountains (northern Morocco). Dense fir forest sectors within Talassemtane National Park (**1**–**3**), showing the characteristic closed-canopy structure of mature *A. marocana* stands; and panoramic view of the Tazaot forest (**4**), where emergent fir trees exceeding 30 m in height and the dark evergreen canopy of *A. marocana* clearly contrast with the surrounding Mediterranean mountain vegetation. Photograph: Rafael Flores Domínguez/RF Natura.

The Moroccan fir is restricted to approximately 4200 ha within Talassemtane National Park (Figure 4) [47,48]. Of this area, around 2450 ha are occupied by pure stands and mixed forest stands dominated by *A. marocana*, reflecting its current structural predominance within the forest mosaic. The species' distribution is geographically organised into two main sectors, corresponding to the Talassemtane and Tazaot fir forests, which together encompass the core of its known range in the Rif Mountains.

The Moroccan fir forests are subject to multiple threats, including deforestation, logging, overgrazing, agricultural expansion, habitat fragmentation, and the resulting population isolation, as well as climate change [4,12,49,50]. In this context, climate change interacts with these pressures, exerting a decisive influence on the regeneration, growth, and future distribution of the species, and shaping vegetation dynamics through changes in phenological patterns [42]. Therefore, analysing long-term changes in the duration and timing of the growing season provides a robust framework for assessing climate-driven phenological shifts in *A. marocana* forests.

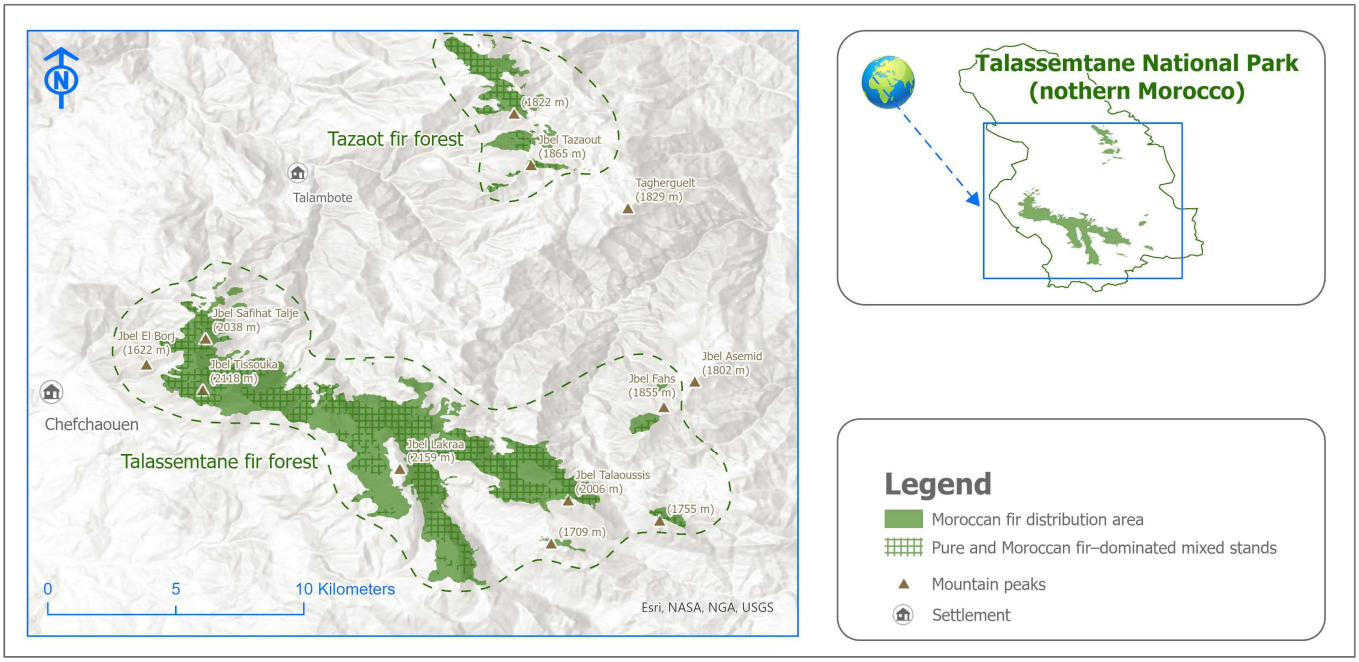


Figure 4. Distribution of the Moroccan fir (*Abies marocana*) in Talassemtane National Park (Northern Morocco). Note: The dashed line delineates the approximate boundaries of the Moroccan fir distribution sectors, corresponding to the Talassemtane and Tazaot fir forests, and is inferred from the spatial aggregation of forest patches. Source: Author's work.

2.2. Remote Sensing Data and GIS Processing

Vegetation dynamics of *A. marocana* forests were analysed using the enhanced vegetation index (EVI) [51] derived from the MOD13Q1 vegetation indices product acquired by the moderate resolution imaging spectroradiometer (MODIS) sensor onboard the Terra satellite. EVI is defined as (Equation (1)):

$$\mathrm{EVI} = G\frac{\rho NIR - \rho RED}{\rho NIR + C_1\rho RED - C_2\rho BLUE + L} \quad (1)$$

where ρNIR, ρRED, and $\rho BLUE$ denote atmospherically corrected surface reflectance in the near-infrared, red, and blue spectral bands, respectively; G is the gain factor (2.5); L is the canopy background adjustment term (1); and C_1 (6.0) and C_2 (7.5) are aerosol resistance coefficients that use the blue band to correct for residual atmospheric contamination.

Compared with the normalised difference vegetation index (NDVI) [52], EVI offers several advantages, particularly relevant for dense Mediterranean mountain forests. First, it reduces saturation effects in closed-canopy environments [53], thereby maintaining sensitivity to interannual variability in vegetation activity. Second, the inclusion of the blue band improves correction for atmospheric influences [54] and minimises background noise arising from soil and rock reflectance—features commonly present in the rugged calcareous terrain of the Rif Mountains. Third, EVI exhibits improved linearity with canopy structural parameters and photosynthetically active vegetation [55], enhancing its suitability for modelling seasonal amplitude and cumulative productivity.

The MOD13Q1 product provides 16-day composite vegetation indices at a spatial resolution of 250 m [55], ensuring temporally regular observations suitable for long-term seasonal modelling and trend detection. It is based on atmospherically corrected surface reflectance data and includes quality assurance (QA) layers that allow the identification of observations affected by clouds, aerosols, or sensor artefacts. Rather than discarding unreliable pixels, anomalous or low-quality values were corrected using harmonic interpo-

lation by fitting a harmonic regression model to each pixel time series [56]. This approach enabled the reconstruction of missing or unreliable observations while preserving the amplitude and phase structure of the seasonal cycle and reducing high-frequency noise without distorting the long-term trend.

The study period extended from January 2000 to December 2024, covering 25 complete calendar years to ensure full annual seasonal cycles. Given the fixed 16-day compositing interval, each year comprises 23 images, resulting in a total of 575 images (23 × 25) across the entire study period. This temporal density provides sufficient resolution to characterise intra-annual seasonal dynamics using harmonic regression approaches [57].

All MODIS tiles covering Talassemtane National Park were spatially masked in a GIS environment using the mapped polygon distribution of *A. marocana* forests. The forest mask was derived from the most recent available cartographic sources, specifically developed for *A. marocana* distribution mapping by Gutiérrez-Hernández [47,58,59], including all areas identified as pure stands or mixed forests with a dominant presence of *A. marocana*. These areas were used to spatially constrain the MODIS analysis during the 2000–2024 study period. In the case of pure stands or forests dominated by *A. marocana*, forest extent was assumed to remain effectively stable over time, although this assumption does not imply ecological or structural stability in forest dynamics.

After quality filtering, harmonic correction, and spatial masking, a total of 655 valid pixels were retained for analysis. Each of these 655 pixels constituted an individual spatial unit for seasonal modelling and subsequent trend testing. Consequently, the statistical framework involved 655 parallel hypothesis tests, forming the basis of the multiple-testing problem explicitly addressed in the methodological section through false discovery rate (FDR) control.

Raster data were imported and formatted in R using the *terra* package [60]. All spatial preprocessing and time-series preparation steps were carried out using the Earth Trends Modeller module developed by the Clark Center for Geospatial Analytics (ClarkCGA) within the TerrSet 2020 (LiberaGIS Version 20.0.4) GIS and remote sensing environment [61]. Subsequent statistical procedures are described in the following section.

2.3. Robust Seasonal Trend Analysis (RSTA)

Seasonal trend analysis (STA) [62] is a sequential analytical framework implemented in the Earth Trends Modeller module of TerrSet [57], which analyses time-series images by estimating temporal trends in seasonal parameters.

Originally, STA performs seasonal trend analysis of time-series images by estimating temporal trends in seasonal parameters derived from intra-annual observations [62,63]. This procedure uses a three-stage time series analysis. First, harmonic regression is applied separately to the intra-annual observations of each pixel for every year in the study period, using all available time-series data to fit yearly seasonal curves and derive seasonal parameters, including amplitude and phase. These parameters characterise the magnitude and timing of the seasonal signal for each year. Second, temporal trends in these yearly parameters are assessed using a nonparametric trend analysis, in which the Theil–Sen estimator is used to quantify the trend magnitude, and the Mann–Kendall test is used to assess its statistical significance. Third, the median slope and intercept values of the harmonic shape parameters are combined within selected regions to reconstruct fitted seasonal curves for the beginning and end of the time series, thereby generating idealised representations of long-term changes in seasonality based on trends estimated across the full study period.

However, the original STA framework does not explicitly account for temporal autocorrelation, spatial dependence among neighbouring pixels, or the increased risk of false

positives arising from multiple testing, since each pixel constitutes a separate trend test. To address these limitations and enhance the robustness of trend detection, we incorporated three additional steps into the second stage of the analysis.

First, we applied an iterative trend-free prewhitening (TFPW) procedure following Wang and Swail [64] to the harmonic parameter time series, which showed significant serial autocorrelation according to the Durbin–Watson test [65,66], thereby reducing first-order temporal dependence while preserving the underlying trend structure prior to trend estimation and significance testing. Second, we applied the contextual Mann–Kendall (CMK) test to account for spatial and cross-correlation between neighbouring pixels, thereby reducing the likelihood of spurious trend detection caused by spatial dependence [67]. Third, we controlled the false discovery rate (FDR) [68] using the Benjamini–Hochberg (BH) procedure, limiting the expected proportion of false positives across the large number of simultaneous tests [69]. These modifications improve the reliability and statistical validity of the detected trends [70]; therefore, the modified procedure is hereafter referred to as robust seasonal trend analysis (RSTA) [33,35].

Finally, fitted seasonal curves representing the beginning and end of the study period were reconstructed from the median slope and intercept values derived from the temporal trends of the harmonic parameters. These curves were displayed only for pixels exhibiting statistically significant trends after contextual Mann–Kendall (CMK) testing and FDR control, and corresponding to areas with pure stands or dominant presence of *A. marocana*, thereby ensuring that the visualised seasonal patterns reflect statistically robust and ecologically meaningful temporal trends.

From these fitted harmonic curves, a comprehensive set of phenological metrics was derived, including mean EVI, peak EVI, seasonal amplitude, and area under the curve (AUC), as well as the seasonal transition metrics green-up date, green-down date, and length of the growing season.

In summary, the complete workflow of the RSTA and phenological metric derivation involved the following steps:

1. Harmonic regression was applied to multi-year intra-annual time series, ensuring that the fitted seasonal parameters for each pixel integrated information from all years and captured the dominant annual and semi-annual components of vegetation seasonality.

2.1. Harmonic parameter time series exhibiting significant serial autocorrelation were corrected using an iterative trend-preserving prewhitening procedure prior to trend estimation and significance testing.

2.2. Temporal trends in the harmonic parameters were quantified using the Theil–Sen (TS) estimator, while statistical significance was assessed using a contextual Mann–Kendall (CMK) test accounting for spatial dependence among neighbouring pixels, followed by false discovery rate (FDR) correction to control for multiple testing across pixels.

3. Seasonal curves representing the beginning and end of the study period were reconstructed from the median slope and intercept values of the harmonic parameters. Phenological metrics were subsequently derived from these fitted curves and visualised only for pixels exhibiting statistically significant trends and corresponding to areas with pure or dominant presence of *A. marocana*.

While the original STA framework was primarily limited to harmonic parameter extraction and robust trend estimation using the Theil–Sen approach, the RSTA framework extends this methodology by incorporating explicit inferential procedures and multiple forms of Type I error control, thereby improving the statistical robustness and reliability of detected phenological trends. Figure 5 summarises the complete analytical workflow, and the mathematical formulations and derivation procedures of the RSTA and the associated phenological metrics are described in detail in the following sections. Additional mathe-

matical details, algorithmic formulations, and methodological developments underlying the workflow are further provided in Supplementary Material S1.

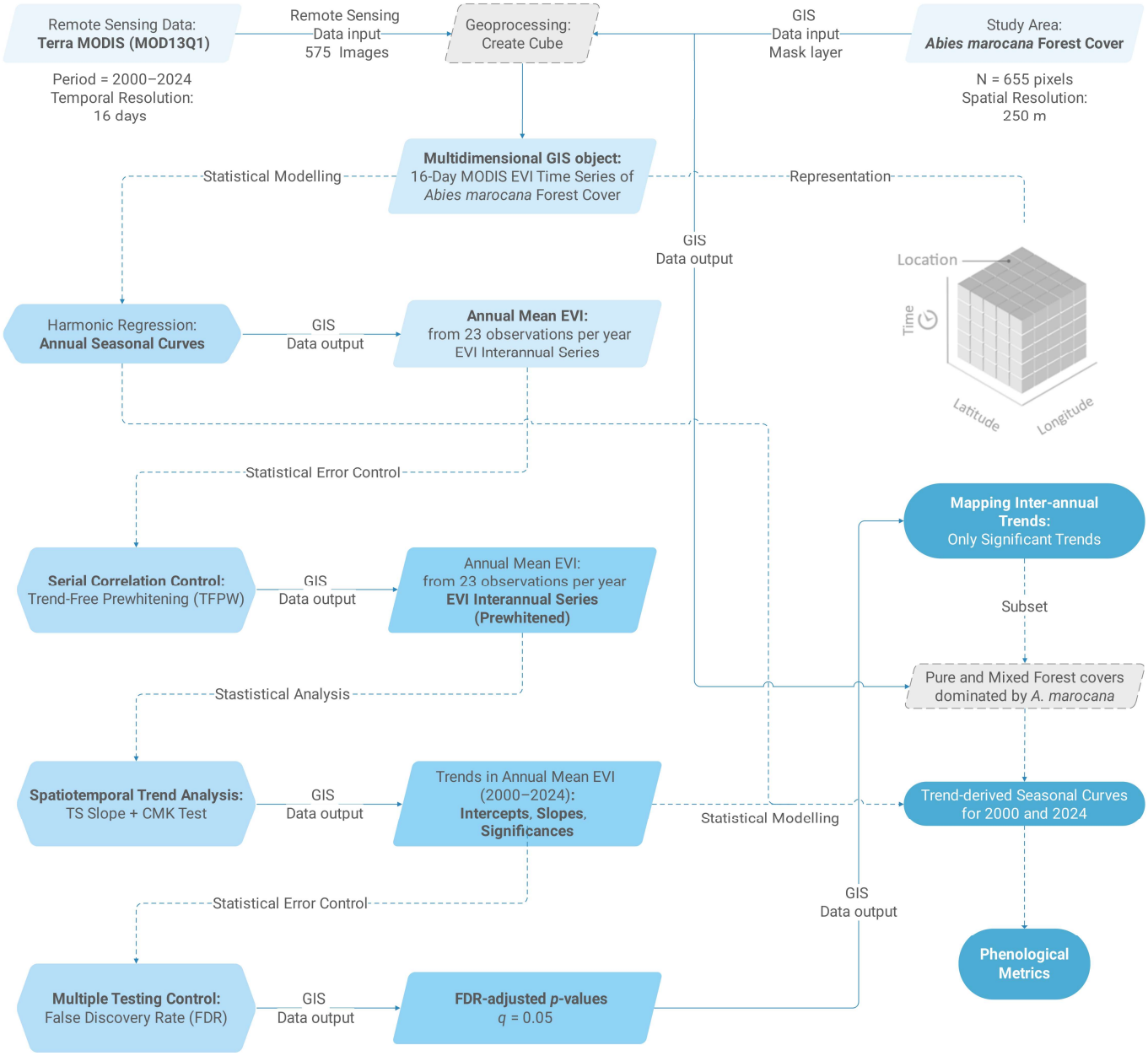


Figure 5. Research workflow diagram of the Robust Seasonal Trend Analysis (RSTA). Trapezoids represent GIS-derived data products, whereas dashed trapezoids indicate spatial subsets generated through masking and geoprocessing operations. Hexagons denote statistical modelling and analytical procedures, and rounded rectangles represent final outputs and derived products. Solid lines indicate GIS data flow between inputs, processing stages, and outputs, whereas dashed lines represent analytical dependencies and statistical relationships among workflow components. Progressive darkening of shaded elements reflects advancing stages of data processing and increasing levels of analytical derivation. Source: Author's work.

2.4. Phenological Metrics

Seasonal metrics for the initial (2000) and final (2024) years were extracted from harmonic regression models fitted to 16-day MODIS EVI time series for all pixels within pure or mixed stands dominated by *A. marocana* that exhibited statistically significant trends after FDR correction.

From the fitted curves, several phenological metrics were derived (Table 1) [71–73], including mean seasonal EVI, peak EVI, seasonal amplitude (defined as the difference between maximum and minimum fitted EVI values), and cumulative seasonal activity, calculated as the area under the fitted seasonal curve (AUC). These metrics provide complementary measures of vegetation productivity, seasonal intensity, and overall ecosystem functioning. Furthermore, seasonal transition dates were characterised using relative amplitude thresholds applied to the harmonic model fitted to the year 2000, which served as the baseline reference; specifically, green-up and green-down were defined as the days of the year when the fitted seasonal curve reached 50% of the seasonal amplitude during the ascending and descending phases, respectively [57,62]. Growing season length was calculated as the interval between green-up and green-down. This model-based definition was preferred over conventional start-of-season (SOS) and end-of-season (EOS) metrics because it provides internally consistent estimates derived from the fitted seasonal trajectory, ensuring robustness to observational noise and comparability under changing seasonal amplitude and productivity conditions.

Table 1. Summary of phenological metrics.

Metric	Description
Mean seasonal EVI	Average value of the fitted EVI curve for each fitted seasonal curve. This metric reflects overall vegetation productivity and mean canopy greenness.
Peak EVI	Maximum value of the fitted seasonal EVI curve, together with its corresponding day of year (DOY). This metric represents the highest level of canopy development and photosynthetic activity during the growing season.
Seasonal amplitude	Difference between the maximum and minimum values of the fitted seasonal EVI curve. This metric quantifies the intensity of seasonal vegetation dynamics and the contrast between dormant and peak conditions.
AUC	Area under the fitted seasonal EVI curve (AUC). This metric represents cumulative vegetation activity and integrates both seasonal duration and productivity.
Centroid of seasonal activity	The centroid of seasonal activity is the DOY representing the centre of mass of the fitted seasonal EVI curve. It indicates when cumulative vegetation activity is temporally centred within the annual cycle.
Green-up	Day of year (DOY) when the fitted seasonal curve reaches 50% of the maximum EVI value of the baseline year (2000) during the ascending phase. This baseline-referenced threshold ensures consistent identification of seasonal onset.
Green-down	Day of year (DOY) when the fitted seasonal curve reaches 50% of the maximum EVI value of the baseline year (2000) during the descending phase. This baseline-referenced threshold ensures consistent identification of seasonal decline.
Growing season length	Number of days between green-up and green-down. This metric represents the duration of active vegetation growth derived from the fitted seasonal trajectory.
Seasonal asymmetry	Seasonal asymmetry measures the imbalance between the ascending and descending phases of the seasonal curve. It reflects whether green-up or senescence dominates the shape of the cycle.
Maximum slope of seasonal increase	The maximum slope of seasonal increase is the steepest rate of rise in fitted EVI during green-up. It indicates how rapidly vegetation accelerates growth at the start of the season.

3. Results

3.1. Evidence of Widespread Significant Greening Across Moroccan Fir Forest Cover

Figure 6 summarises the distribution of discoveries and non-discoveries obtained from the contextual Mann–Kendall (CMK) trend test applied to annual mean EVI over Moroccan fir forests, comparing analyses performed with and without prewhitening (PW-CMK). Using an unadjusted significance threshold of $\alpha = 0.05$, the CMK analysis identified 566 discoveries (86.4%), whereas the PW-CMK approach identified 530 discoveries (80.9%), reflecting the more conservative behaviour expected when accounting for temporal autocorrelation. After applying the Benjamini–Hochberg false discovery rate correction (FDR-BH, $q = 0.05$), the number of discoveries decreased slightly to 562 (85.8%) and 519 (79.2%) for CMK and PW-CMK, respectively. Despite this reduction, the overall balance between discoveries and non-discoveries remained largely unchanged.

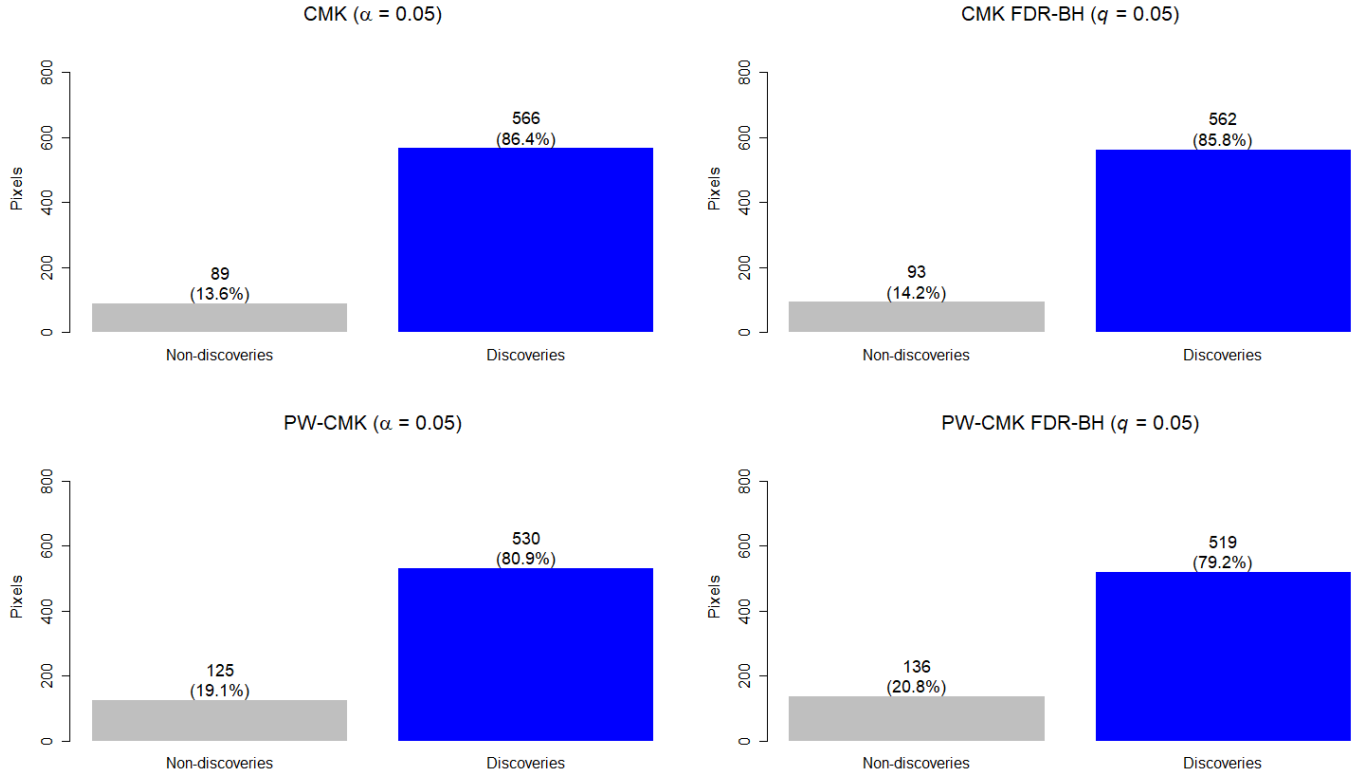


Figure 6. Distribution of the significant trends (discoveries) and non-significant results (non-discoveries) detected by the contextual Mann–Kendall (CMK) tests applied to annual mean EVI over Moroccan fir forests in the Rif region, comparing analyses performed with and without prewhitening (PW-CMK). Left panels correspond to discoveries obtained from unadjusted *p*-values ($\alpha = 0.05$), whereas right panels show discoveries retained after Benjamini–Hochberg false discovery rate correction (FDR-BH, $q = 0.05$). Bar heights represent the number of pixels, while percentages indicate their proportion relative to the total number of valid pixels. In the terminology of false discovery rate (FDR) control, a "discovery" refers to a rejected null hypothesis, irrespective of whether multiplicity correction is applied. Source: Author's work.

Figure 7 maps the spatial distribution of discoveries obtained from the contextual Mann–Kendall (CMK) trend test applied to annual mean EVI over Moroccan fir forests, comparing analyses performed with and without prewhitening (PW-CMK). In both approaches, discoveries were concentrated mainly within the core fir stands of Talassemtane and Tazaot. Applying the Benjamini–Hochberg false discovery rate (FDR) correction ($q = 0.05$) produced only minor spatial changes relative to the unadjusted results ($\alpha = 0.05$), mostly affecting peripheral and fragmented areas. Compared with the standard CMK

analysis, the PW-CMK approach yielded a slightly more conservative spatial pattern, with fewer discoveries in marginal zones.

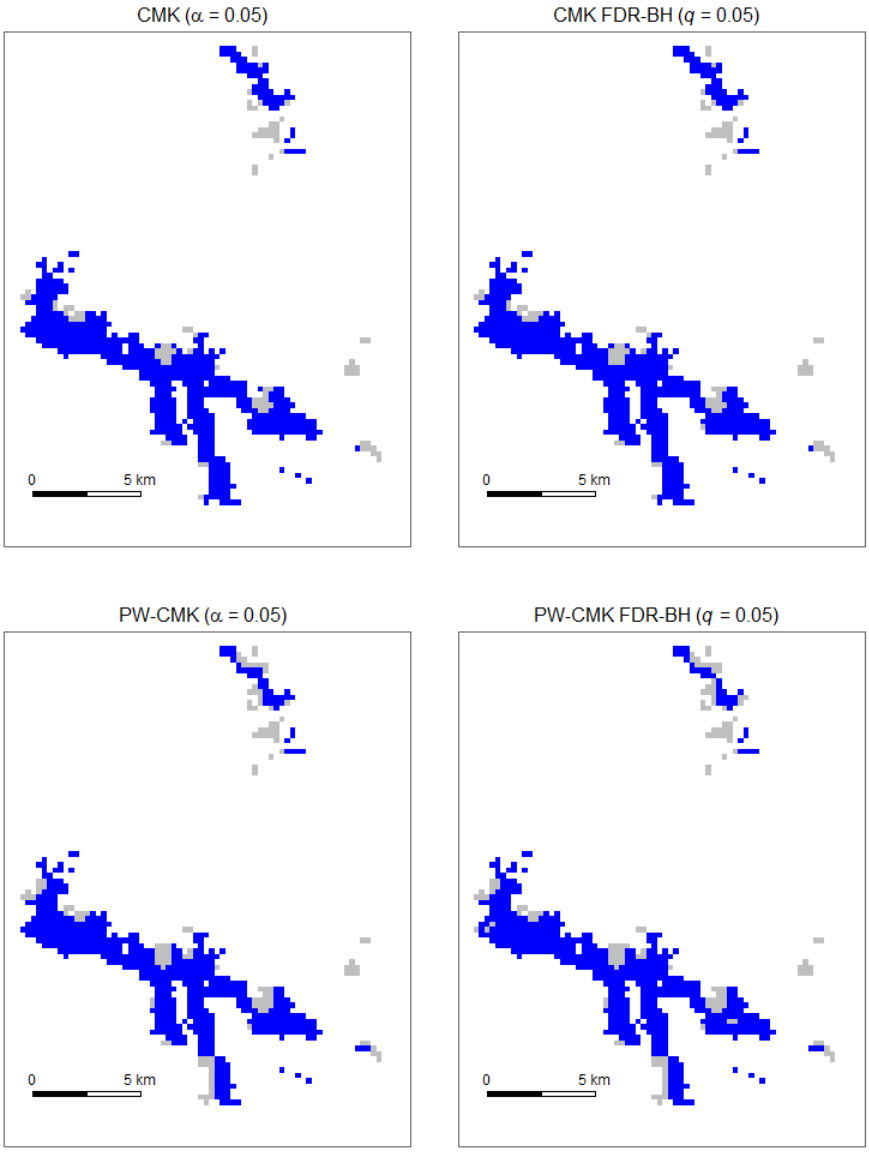


Figure 7. Mapping the distribution of significant trends (discoveries) and non-significant results (non-discoveries) detected by the contextual Mann–Kendall (CMK) trend tests applied to interannual mean EVI in Moroccan fir forests, comparing analyses performed with and without prewhitening (PW-CMK). Left panels correspond to discoveries obtained from unadjusted p-values ($\alpha = 0.05$), whereas right panels show discoveries retained after Benjamini–Hochberg false discovery rate correction (FDR-BH, $q = 0.05$). Blue pixels represent discoveries, whereas grey pixels indicate non-discoveries. In the terminology of false discovery rate (FDR) control, a "discovery" refers to a rejected null hypothesis, irrespective of whether multiplicity correction is applied. Source: Author's work.

Supplementary Material S2 presents additional results obtained using alternative significance thresholds ($\alpha/q = 0.10$ and $\alpha/q = 0.01$) for both CMK and PW-CMK approaches, before and after FDR-BH correction. The threshold of 0.10 is relatively common in environmental trend analyses, whereas 0.01 is substantially more conservative. Overall, the main spatial patterns and proportions of discoveries remained broadly consistent across thresholds, although the strongest reduction in discoveries was associated with the PW-CMK approach rather than with FDR-BH correction, particularly in edge areas and within the Tazaot fir forest.

Figure 8 maps the distribution of Theil–Sen slope values in the Moroccan fir forest. Positive slopes (greening) clearly predominated across the study area: among the 655 valid pixels, 632 (≈96.5%) showed positive trends, whereas only 23 (≈3.5%) showed negative trends (browning). Of the 519 pixels previously identified as significant (discoveries) after prewhitening of the time series and subsequent Benjamini–Hochberg false discovery rate correction of the CMK results (PW-CMK FDR-BH, $q = 0.05$), all exhibited positive slopes. No significant negative slopes remained after multiple-testing correction.

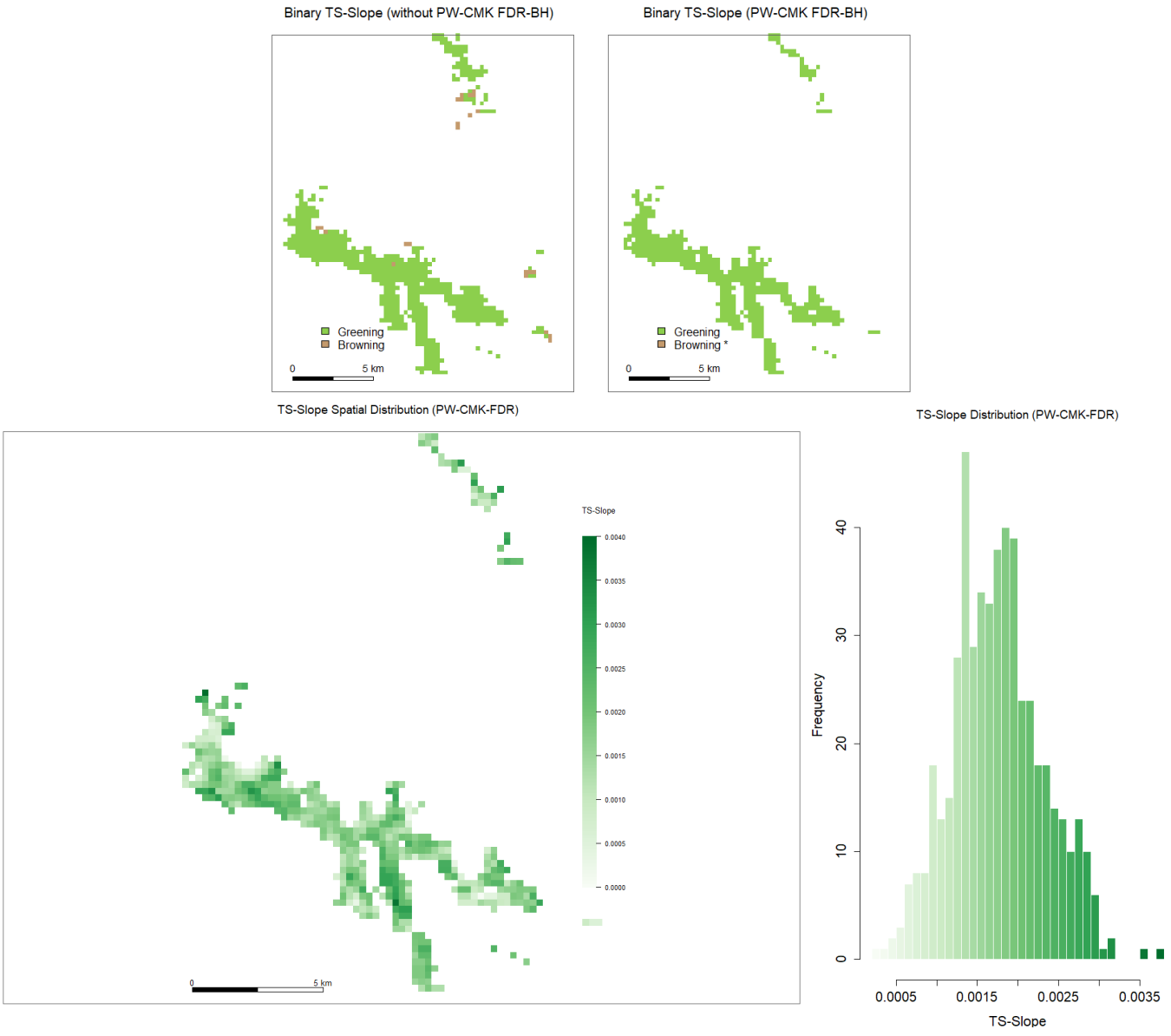


Figure 8. Mapping the distribution of Theil–Sen slope directions and magnitudes derived from interannual mean EVI in Moroccan fir forests. The (**upper-left**) map shows the signs of monotonic trends estimated from the standard Theil–Sen slope (TS-Slope), whereas the (**upper-right**) map shows slopes retained after prewhitening and filtering using the contextual Mann–Kendall procedure with Benjamini–Hochberg false discovery rate correction (PW-CMK FDR-BH, $q = 0.05$). Green pixels indicate greening trends (positive slopes), whereas brown pixels indicate browning trends (negative slopes). The asterisk (*) accompanying "Browning" in the PW-CMK FDR-BH map indicates that no significant negative slopes were detected after false discovery rate correction. The lower panel shows the spatial distribution of significant PW-CMK FDR-BH Theil–Sen slopes (**lower-left**) and the corresponding frequency distribution histogram (**lower-right**), both represented using a continuous green gradient proportional to slope magnitude. Source: Author's work.

Significant Theil–Sen slope values ranged from approximately 0.00025 to 0.00374 EVI year^{-1}. The close similarity between the mean (≈0.00175) and median (≈0.00174), together with the moderate interquartile range (Q1 ≈ 0.00138; Q3 ≈ 0.00212), indicates a relatively homogeneous distribution of intermediate positive slope magnitudes across the study area. The absence of significant negative slopes after prewhitening and FDR correction further supports the interpretation that the observed increase in EVI represents a robust spatial signal rather than a pattern driven by local fluctuations or temporal noise. Although a few pixels exhibited comparatively high slopes (>0.003), these appear to represent isolated cases within a broader pattern of moderate and widespread greening.

3.2. Intensification and Extension of the Growing Season

The fitted seasonal EVI trajectories derived from harmonic regression within the RSTA framework revealed pronounced phenological changes between 2000 and 2024 in pure and mixed forest stands dominated by *A. marocana* (Figure 9; Table 2). These trajectories represent the modelled seasonal dynamics of the initial and final years of the 2000–2024 prewhitened EVI time series and were reconstructed exclusively from pixels exhibiting statistically significant seasonal trends after contextual Mann–Kendall (CMK) testing and Benjamini–Hochberg false discovery rate (FDR) correction. Consequently, the patterns described below correspond to statistically robust regional patterns rather than isolated local variability.

Table 2. Changes in Seasonal Vegetation Metrics (2000–2024).

Metric	2000	2024	Change
Mean EVI	0.245	0.286	+0.041
Peak EVI	0.337	0.387	+0.050
Seasonal amplitude	0.163	0.186	+0.023
AUC	83.22	95.82	+12.60
Green-up (DOY)	120	96	−24 days
Green-down (DOY)	266	290	+24 days
Growing season length (days)	146	194	+48 days

The fitted trajectories showed a generalised increase in EVI values throughout nearly the entire annual cycle, indicating that the detected changes were not restricted to peak seasonal productivity alone, but reflected a broader enhancement of vegetation activity across most months of the year. Mean EVI increased from 0.249 in 2000 to 0.287 in 2024 (+15.2%), while minimum EVI increased from 0.175 to 0.201 (+15.0%) and peak EVI rose from 0.338 to 0.388 (+14.8%). Seasonal amplitude increased from 0.163 to 0.187 (+14.6%), and cumulative seasonal activity, quantified as the area under the curve (AUC), increased from 83.23 to 95.85 (+15.2%). In parallel, the maximum seasonal green-up slope increased from 0.00197 to 0.00223 EVI day−1 (+13.1%), suggesting a slightly steeper seasonal activation phase. Collectively, these changes indicate a substantial intensification of canopy greenness and seasonal vegetation activity over the 25-year study period.

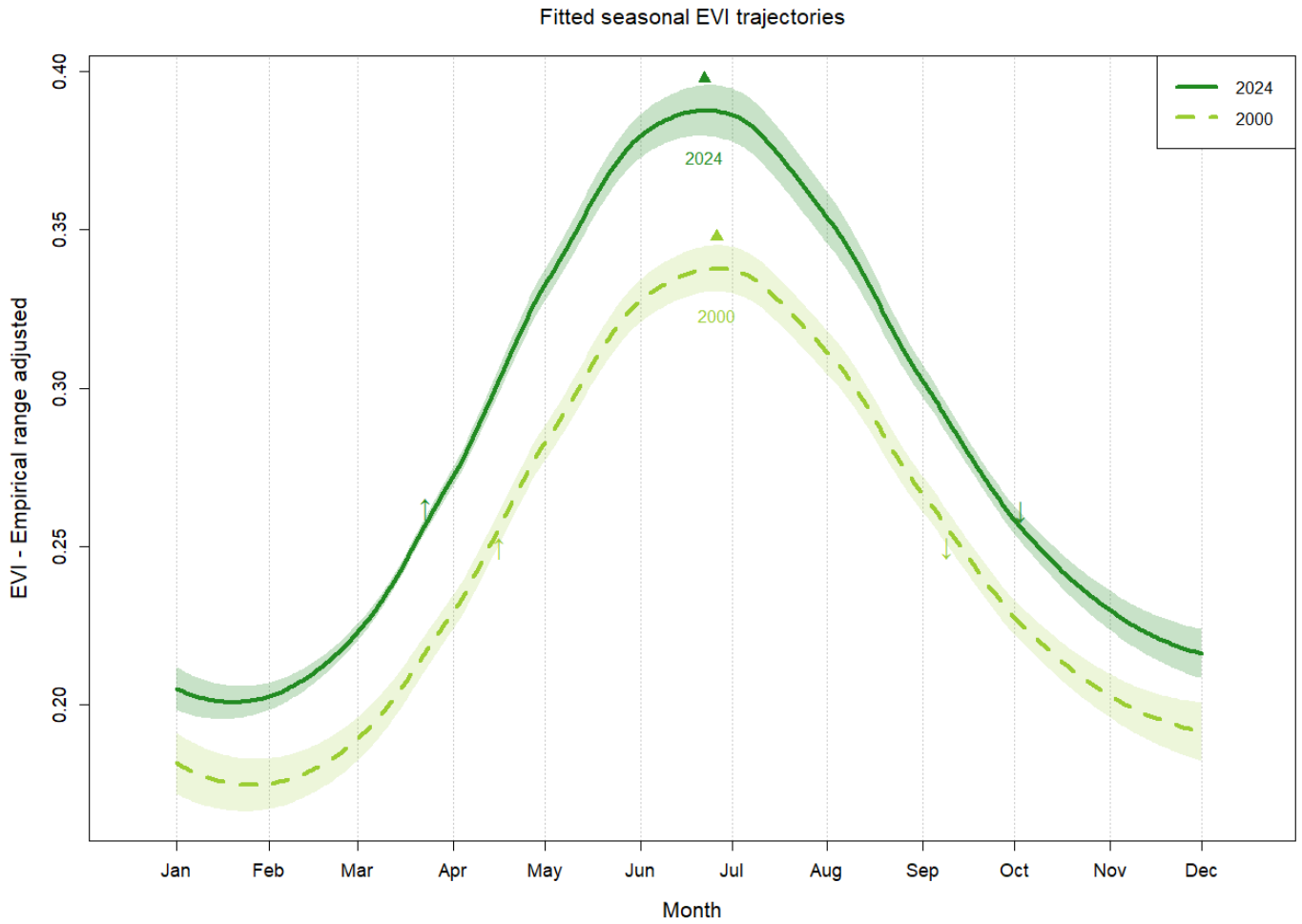


Figure 9. Modelled seasonal curves of pure and mixed forest stands dominated by *Abies marocana* from 2000 to 2024 (25 years). Note: Fitted seasonal EVI trajectories were reconstructed from the median slope and intercept values derived from temporal trends in harmonic parameters within the robust seasonal trend analysis (RSTA) framework. Curves were generated exclusively from pixels exhibiting statistically significant seasonal trends after contextual Mann–Kendall (CMK) testing and Benjamini–Hochberg false discovery rate (FDR) correction (q = 0.05), and corresponding to pure stands or mixed stands with dominant presence of *A. marocana*. The dark green solid line represents the fitted trajectory for 2024, whereas the lighter green dashed line represents the fitted trajectory for 2000. Shaded ribbons around each trajectory represent empirical 95% confidence intervals derived from variability among fitted curves. Triangles indicate the seasonal peak (maximum EVI) for each year, while arrows denote green-up and green-down dates estimated using the 50% relative amplitude threshold. EVI values correspond to empirical range-adjusted MODIS Terra MOD13Q1 data (16-day composite, 250 m spatial resolution). Source: Author's work.

Seasonal land surface phenology also shifted markedly. When phenological thresholds were defined using the 50% relative amplitude criterion applied to the fitted harmonic trajectories, the estimated onset of the growing season (green-up) advanced by 24 days, shifting from DOY 120 in 2000 to DOY 96 in 2024. In contrast, the estimated end of the growing season (green-down) was delayed by 24 days, from DOY 266 to DOY 290. Consequently, the modelled growing season length increased from 146 to 194 days (+48 days; +32.9%), indicating a substantially longer period of sustained photosynthetic activity. Despite these marked changes in seasonal boundaries, the centroid of annual EVI activity remained comparatively stable (DOY 187–186), suggesting that the detected phenological change primarily reflected an expansion and intensification of seasonal activity around a relatively stable annual centre of vegetation functioning.

The empirical confidence intervals associated with the fitted trajectories indicated that uncertainty was comparatively greater at the beginning and end of the annual cycle, where EVI values are lower, and variability among reconstructed trajectories is proportionally higher. In contrast, the green-up and green-down phases exhibited comparatively narrower confidence intervals, suggesting that the timing of the main phenological transitions was relatively consistent across reconstructed trajectories. Collectively, these results indicate a coherent regional tendency towards enhanced vegetation activity, earlier spring activation, delayed seasonal senescence, and a substantial extension of the annual period of ecological functioning in *A. marocana* forest stands.

4. Discussion

Our results reveal a statistically significant increasing trend in vegetation activity and growing-season length in *A. marocana* forests over the 2000–2024 period. Significant increases in mean EVI were observed across most areas—operationally represented as pixels—within the main forest masses of Talassemtane and Tazaot, indicating marked increases in vegetation activity in consolidated forest stands. By contrast, areas exhibiting non-significant negative trends in mean EVI are mainly restricted to forest edges, fragmented areas, or sectors affected by recent disturbance [49,50].

Beyond the increase in annual mean EVI, harmonic modelling of seasonality shows a substantial intensification of vegetation activity across the annual cycle in pure stands or stands dominated by *A. marocana*. The seasonal curves shown for 2000 and 2024 are derived from the harmonic regression applied to the complete time series (2000–2024), ensuring internal coherence and stability in the estimation of seasonal parameters throughout the study period. Furthermore, the seasonal curves correspond exclusively to pixels exhibiting statistically significant seasonal trends after the FDR correction, so that the trends described reflect only spatially and statistically robust patterns [33]. The simultaneous increase in mean EVI, seasonal peak, amplitude, and AUC indicates that not only are higher levels of vegetation activity reached at the time of maximum productivity, but cumulative activity throughout the year is also markedly greater. Vegetation indices such as EVI are strongly linked to canopy structure, leaf area, and photosynthetic activity, and their integrated seasonal values provide reliable proxies of ecosystem productivity and functioning [74,75]. This pattern points to a functional intensification of the forest landscape system, potentially associated with an effective extension of photosynthetic activity and/or structural changes in the canopy, such as increases in leaf density or canopy continuity. Similar increases in integrated vegetation activity have been interpreted as indicators of enhanced ecosystem productivity and carbon uptake [75]. Taken together, these results suggest a strengthening of the productive signal in stands dominated by *A. marocana*, rather than a simple fluctuation in maximum annual values. Nevertheless, although the analysis focused on persistent forest stands with confirmed *A. marocana* presence, the potential influence of local disturbance dynamics or structural recovery processes cannot be entirely excluded in some areas (pixels).

Trends in the length of the growing season are also among the most relevant outcomes of the seasonal analysis (Figure 9). The earlier green-up, together with the delay in green-down, results in a substantial prolongation of the annual period of vegetation activity. This bidirectional expansion is consistent with widespread phenological responses to climate warming, which have been extensively documented using satellite observations and ground-based measurements [76,77]. Warmer spring temperatures promote earlier vegetation activation, while milder autumn conditions delay senescence, effectively extending the duration of photosynthetic activity and ecosystem functioning [78,79]. These patterns are particularly evident in montane environments, where vegetation phenology is

strongly constrained by temperature [80,81]. Importantly, these patterns should be interpreted within the framework of reconstructed land-surface phenology derived from EVI trajectories, reflecting integrated seasonal dynamics of vegetation activity at the forest-level rather than direct organism-level phenological observations [19].

Similar patterns have been documented in *Abies pinsapo* forests [44] and in other Mediterranean mountain ecosystems [35], where earlier spring onset and extended vegetation activity have been linked to recent increases in temperature [82]. The stability of the seasonal centroid suggests that the central period of maximum productivity remains relatively constant within the annual calendar, while the initial and final margins of the growing season exhibit progressive shifts [83,84]. The change in seasonal asymmetry and the increase in the maximum slope of the fitted curve further point to a trend toward more rapid spring development, indicating an acceleration of the cycle's ascending phase rather than a uniform amplification of the seasonal pattern [71]. However, from a methodological perspective, it is important to acknowledge potential geometric sensitivities inherent to threshold-based definitions of the growing season [84]. The green-up and green-down were defined using a 50% relative amplitude criterion applied to fitted harmonic curves. Because this threshold is expressed relative to annual amplitude, changes in curve shape—including shifts in asymmetry or variations in higher-order harmonic components—may influence the timing of threshold crossings. Although a purely vertical amplification of the seasonal curve would not alter the timing of the 50% relative threshold, modifications in curvature or the rate of seasonal transition could alter the estimated growing-season length [85]. In addition, confidence intervals associated with the reconstructed trajectories tended to widen at lower EVI levels, particularly near the onset and termination of seasonal activity, supporting the use of an intermediate threshold as a comparatively more stable reference level [86]. Nevertheless, alternative approaches based on adaptive thresholds or derivative-derived transition metrics could provide additional insight into the sensitivity of reconstructed phenological estimates and warrant future evaluation. Therefore, part of the observed extension may reflect structural changes in the modelled seasonal profile rather than a strictly biological phenological shift [84]. However, the concurrent advancement of peak timing, increase in maximum slope, and rise in cumulative seasonal activity collectively support the interpretation of a substantive reorganisation of seasonal dynamics rather than a methodological artefact [84].

In the broader context of Mediterranean mountain ecosystems, these trends should be interpreted with caution. In high-elevation forest environments where relatively low temperatures have historically constrained growth, recent warming may initially enhance vegetation activity by reducing thermal limitation and extending the effective photosynthetic period [87,88]. Under such conditions, increased seasonal activity and a longer growing season may translate into higher annual carbon uptake and more pronounced canopy development [89]. Consequently, increasing EVI trends should not be interpreted as unequivocal evidence of improved ecosystem condition or long-term resilience [90]. In Mediterranean climates characterised by marked summer drought, a prolonged growing season may also lead to greater cumulative water demand [91], potentially increasing vulnerability to extended dry spells or extreme heat events. The balance between potential thermal benefits and hydric constraints will therefore be critical in determining whether the observed greening represents a sustained shift in ecosystem functioning or a transient phase preceding heightened stress [90,92], disturbance, and increased wildfire risk under future climatic scenarios [93].

From a methodological standpoint, integrating harmonic seasonal modelling with trend-free prewhitening to reduce serial autocorrelation in interannual trends, robust nonparametric trend estimators, and false discovery rate control provides a statistically

sound basis for interpreting the detected trends [35,92]. The persistence of the greening signal following FDR correction indicates that the observed patterns do not arise from spurious significance generated by multiple simultaneous tests but instead reflect spatially coherent and statistically reliable trends [94]. This aspect is particularly relevant in pixel-level remote sensing analyses [70], where the large number of parallel hypothesis tests may inflate Type I error rates if multiplicity is not properly addressed [36,39].

Nevertheless, the present study has several limitations that should be considered when interpreting the results. First, EVI serves as an indirect spectral proxy for vegetation activity and does not allow precise discrimination between structural canopy changes, physiological variations in photosynthetic efficiency, or shifts in species composition [95]. Consequently, part of the detected greening signal may also reflect local structural recovery or progressive canopy densification within persistent forest stands, rather than exclusively phenological processes [96]. In addition, the 250 m spatial resolution may integrate substantial internal heterogeneity within each pixel, particularly in transition zones between pure and mixed stands or in areas affected by local disturbances [97]. To preserve the original spatial structure of the MODIS data and avoid visually misleading artefacts, all trend maps were represented directly from the original raster outputs without bilinear interpolation or spatial smoothing. In this sense, the detected trends should not be interpreted strictly as phenological changes in a biological sense [98], since processes operating at different scales—structural, demographic, or landscape-dynamic—may influence the observed spectral signal. In addition, no independent validation using alternative datasets such as MODIS LAI, SIF products, field phenology, or high-resolution fractional vegetation cover was performed, which should be considered when interpreting subtle phenological signals in evergreen conifer systems [99]. Although MODIS Collection 6.1 substantially improves temporal consistency, residual platform-related effects associated with Terra MODIS orbit drift and long-term sensor calibration cannot be entirely excluded, particularly when analysing subtle long-term vegetation trends [100]. Future Terra–Aqua comparative analyses, cross-sensor comparisons, or the integration of combined MODIS products could further improve the robustness of long-term phenological assessments. Moreover, the analysis does not explicitly incorporate climatic variables or indicators of water availability, which limits direct causal attribution of the identified trends.

Future research should therefore integrate climatic time series, including ERA5-Land datasets, drought indices, explicit phenology–climate coupling analyses, and dendroecological or ecophysiological data to better elucidate the mechanisms underlying the observed trends [101]. It may also prove particularly valuable to conduct higher-resolution analyses using satellite programs such as Landsat [102], working at the stand level or even on selected plots, thereby reducing within-pixel heterogeneity and improving the structural and phenological interpretation of the signal [103]. Such approaches could additionally facilitate analyses of topographic and structural gradients, including elevation, aspect, and forest composition effects on long-term seasonal dynamics, while incorporating independent validation datasets (e.g., LAI, SIF, or field-based observations), pixel-wise uncertainty propagation, and probabilistic phenological simulations, particularly in evergreen conifer systems where phenological signals derived from vegetation indices may be comparatively subtle [101]. They could also help evaluate the sensitivity of reconstructed seasonal trajectories to alternative harmonic configurations and complementary vegetation indices or BRDF-corrected products (e.g., EVI2 or NBAR-derived datasets), especially in mountainous environments where aerosol and topographic effects may influence long-term spectral consistency [104]. Such an approach would additionally enable direct comparisons with *A. pinsapo* forests in southern Iberia, contributing to a biogeographical assessment of the responses of these closely related relict taxa to recent warming [58]. Continued monitoring

under scenarios of increasing aridity and more frequent extreme events will, in any case, be essential to determine whether the current trends of seasonal intensification and extension persist or give way to heightened vulnerability in the medium to long term [105].

5. Conclusions

Moroccan fir forests have shown statistically significant trends of intensified vegetation activity and extended growing seasons over the 2000–2024 period. The magnitude of the reconstructed seasonal expansion relative to productivity gains indicates that temporal extension of seasonal activity represents a central component of the detected greening signal. Particularly evident in pure and *A. marocana*-dominated stands, these patterns are consistent with warming-related responses commonly reported in Mediterranean mountain ecosystems.

Robust Seasonal Trend Analysis (RSTA) combines harmonic regression, iterative trend-free prewhitening (TFPW) following Wang and Swail, Theil–Sen (TS) slope estimation, the contextual Mann–Kendall (CMK) test, and false discovery rate (FDR) correction, providing a robust framework for assessing spatially explicit seasonal dynamics. By explicitly accounting for serial autocorrelation in interannual trends, spatial dependence, and multiple testing, this approach reduces the likelihood that the observed trends arise from spurious pixel-level significance and strengthens confidence in the inferential robustness of the detected patterns.

However, the ecological implications of this seasonal intensification remain context-dependent. While reduced thermal limitation at high elevations may initially stimulate vegetation activity, prolonged growing seasons could also increase cumulative water demand in this drought-prone region. Under such conditions, enhanced seasonal productivity does not necessarily translate into long-term resilience. Continued monitoring, climatic attribution analyses, independent validation datasets, and higher-resolution comparative approaches will therefore be essential to determine whether the observed reorganisation of seasonal dynamics represents sustained functional adjustment or a transitional phase preceding heightened vulnerability under continued warming.

Supplementary Materials: The following supporting information can be downloaded at: https://www.mdpi.com/article/10.3390/rs18122052/s1. There are two Supplementary Materials associated with this manuscript: Supplementary Material S1 (Mathematical Details of the Robust Seasonal Trend Analysis (RSTA)) and Supplementary Material S2 (Additional information related to Figures 6 and 7). The final versions of both supplementary materials have been provided in PDF format. Figure S1. Distribution of significant trends ("discoveries") and non-significant pixels detected from annual mean EVI in Moroccan fir forests (Rif Mountains, Morocco) under the four analytical configurations: CMK (contextual Mann–Kendall test applied directly), PW-CMK (CMK applied to prewhitened time series), CMK-FDR (CMK with false discovery rate correction), and PW-CMK-FDR (prewhitened CMK with FDR correction). Significance thresholds were set at $\alpha = 0.10$ (uncorrected tests) and $q = 0.10$ (FDR-adjusted results). Figure S2. Distribution of significant trends ("discoveries") and non-significant pixels detected from annual mean EVI in Moroccan fir forests (Rif Mountains, Morocco) under the four analytical configurations: CMK (contextual Mann–Kendall test applied directly), PW-CMK (CMK applied to prewhitened time series), CMK-FDR (CMK with false discovery rate correction), and PW-CMK-FDR (prewhitened CMK with FDR correction). Significance thresholds were set at $\alpha = 0.01$ (uncorrected tests) and $q = 0.01$ (FDR-adjusted results).

Author Contributions: Conceptualisation: O.G.-H.; Methodology: O.G.-H. and L.V.G.; Software: O.G.-H.; Formal analysis: O.G.-H.; Investigation: O.G.-H.; Data curation: O.G.-H.; Project administration: O.G.-H. and L.V.G.; Visualisation: O.G.-H.; Writing—original draft preparation: O.G.-H.; Writing—review and editing: O.G.-H. and L.V.G. All authors have read and agreed to the published version of the manuscript.

Funding: This investigation contributes to the projects PALEONIEVES (ref. 3025/2023) and PALEOPINSAPO II (ref. PID2022-141592NB-I00). The APC was waived by the publisher.

Data Availability Statement: The complete data set supporting the findings of this study is available from the corresponding author, O.G.-H.

Acknowledgments: The authors sincerely thank the three anonymous reviewers for their thorough, constructive, and intellectually challenging comments, which substantially strengthened the manuscript, improving its scientific clarity, study design, presentation of results, and several aspects of the discussion. The authors also gratefully acknowledge Rafael Flores Domínguez (RF Natura) for providing the photographs used in Figure 3.

Conflicts of Interest: The authors declare no conflicts of interest.

References

1. Trabut, L. Sur La Présence d'un *Abies* Nouveau Au Maroc (*Abies marocana*). *Bull. De La Société Bot. De Fr.* **1906**, *53*, 154–155. [CrossRef]
2. Trabut, L. Le Sapin Du Maroc. *Abies Marocana* Trab. (Soc. Bot. Fr., 1906). *Bull. De La Société Bot. De Fr.* **1928**, *75*, 897–902. [CrossRef]
3. Linares, J.C. Biogeography and Evolution of Abies (*Pinaceae*) in the Mediterranean Basin: The Roles of Long-Term Climatic Change and Glacial Refugia. *J. Biogeogr.* **2011**, *38*, 619–630. [CrossRef]
4. Ben-Said, M.; El Aich, N.; Berrad, F.; Ghallab, A. Knowledge Status of the Endemic Moroccan Fir Forest (*Abies marocana* Trab.): Achievements, Gaps, and New Research Axes. *Bull. De L'institut Sci. Rabat Sect. Sci. De La Vie* **2024**, *46*, 1–16. Available online: https://portal.issn.org/resource/ISSN/2458-7184 (accessed on 19 May 2026). [CrossRef]
5. Aussenac, G. Ecology and Ecophysiology of Circum-Mediterranean Firs in the Context of Climate Change. *Ann. For. Sci.* **2002**, *59*, 823–832. [CrossRef]
6. Caudullo, G.; Tinner, W. *Abies*–Circum-Mediterranean Firs in Europe: Distribution, Habitat, Usage and Threats. In *European Atlas of Forest Tree Species*; European Commission: Brussels, Belgium, 2016; p. e01e1b6+. Available online: https://forest.jrc.ec.europa.eu/media/atlas/Abies_spp.pdf (accessed on 19 May 2026).
7. Ben-Said, M. The Taxonomy of Moroccan Fir *Abies marocana* Trab. (*Pinaceae*): Conceptual Clarifications from Phylogenetic Studies. *Mediterr. Bot.* **2022**, *43*, e71201. [CrossRef]
8. Dering, M.; Sekiewicz, K.; Boratyńska, K.; Litkowiec, M.; Iszkuło, G.; Romo, A.; Boratyński, A. Genetic Diversity and Inter-Specific Relations of Western Mediterranean Relic *Abies* Taxa as Compared to the Iberian *A. Alba*. *Flora Morphol. Distrib. Funct. Ecol. Plants* **2014**, *209*, 367–374. [CrossRef]
9. Ben-Said, M.; Ghallab, A.; Lamrhari, H.; Carreira, J.A.; Linares, J.C.; Taïqui, L. Characterizing Spatial Structure of *Abies marocana* Forest through Point Pattern Analysis. *For. Syst.* **2020**, *29*, e014. [CrossRef]
10. Benabid, A. *Flore et Écosystèmes Du Maroc. Évaluation et Préservation de La Biodiversité*; Éditions Ibis Press: Paris, France, 2000.
11. Alaoui, A.; Laaribya, S.; Ayan, S.; Ghallab, A.; López-Tirado, J. Modelling Spatial Distribution of Endemic Moroccan Fir (*Abies marocana* Trabut) in Talassemtane National Park, Morocco. *Austrian J. For. Sci.* **2021**, *138*, 73–94. Available online: https://www.forestscience.at/artikel/2021/02/modelling-spatial-distribution-of-endemic-moroccan-fir.html (accessed on 19 May 2026).
12. Ben-Said, M.; Sakar, E.H. A Systematic Review on the Endemic Moroccan Fir (*Abies marocana* Trab.) and Its Implications for Conservation and Future Research Perspectives. *Folia Geobot.* **2023**, *58*, 31–53. [CrossRef]
13. Hatzilazarou, S.; El Haissoufi, M.; Pipinis, E.; Kostas, S.; Libiad, M.; Khabbach, A.; Lamchouri, F.; Bourgou, S.; Megdiche-Ksouri, W.; Ghrabi-Gammar, Z.; et al. GIS-Facilitated Seed Germination and Multifaceted Evaluation of the Endangered *Abies marocana* Trab. (*Pinaceae*) Enabling Conservation and Sustainable Exploitation. *Plants* **2021**, *10*, 2606. [CrossRef] [PubMed]
14. Eamus, D.; Huete, A.; Yu, Q. *Vegetation Dynamics. A Synthesis of Plant Ecophysiology, Remote Sensing and Modelling*; Cambridge University Press: Cambridge, UK, 2016.
15. Pettorelli, N.; Vik, J.O.; Mysterud, A.; Gaillard, J.M.; Tucker, C.J.; Stenseth, N.C. Using the Satellite-Derived NDVI to Assess Ecological Responses to Environmental Change. *Trends Ecol. Evol.* **2005**, *20*, 503–510. [CrossRef] [PubMed]
16. Clarivate Analytics. *Research Fronts 2020*; Clarivate Analytics: London, UK, 2021; Available online: https://discover.clarivate.com/ResearchFronts2020_ENhttps://discover.clarivate.com/ResearchFronts2020_EN (accessed on 19 May 2026).
17. Kuenzer, C.; Dech, S.; Wagner, W. (Eds.) *Remote Sensing Time Series*; Springer International Publishing: Cham, Switzerland, 2015; Volume 22. [CrossRef]
18. Schwartz, M.D. (Ed.) *Phenology: An Integrative Environmental Science*; Springer: Dordrecht, The Netherlands, 2013.
19. Helman, D. Land Surface Phenology: What Do We Really 'See' from Space? *Sci. Total Environ.* **2018**, *618*, 665–673. [CrossRef] [PubMed]

20. Roerink, G.J.; Menenti, M.; Soepboer, W.; Su, Z. Assessment of Climate Impact on Vegetation Dynamics by Using Remote Sensing. *Phys. Chem. Earth* **2003**, *28*, 103–109. [CrossRef]
21. Park, J.S.; Post, E. Seasonal Timing on a Cyclical Earth: Towards a Theoretical Framework for the Evolution of Phenology. *PLoS Biol.* **2022**, *20*, e3001952. [CrossRef] [PubMed]
22. Urdiales-Flores, D.; Zittis, G.; Hadjinicolaou, P.; Osipov, S.; Klingmüller, K.; Mihalopoulos, N.; Kanakidou, M.; Economou, T.; Lelieveld, J. Drivers of Accelerated Warming in Mediterranean Climate-Type Regions. *npj Clim. Atmos. Sci.* **2023**, *6*, 97. [CrossRef]
23. Qadem, Z.; Tayfur, G. In-Depth Exploration of Temperature Trends in Morocco: Combining Traditional Methods of Mann Kendall with Innovative ITA and IPTA Approaches. *Pure Appl. Geophys.* **2024**, *181*, 2717–2739. [CrossRef]
24. Cuttelod, A.; García, N.; Abdul Malak, D.; Temple, H.; Katariya, V. The Mediterranean: A Biodiversity Hotspot under Threat. In *The 2008 Review of The IUCN Red List of Threatened Species*; IUCN: Gland, Switzerland, 2008. Available online: https://iucn.org/sites/default/files/import/downloads/the_mediterranean_a_biodiversity_hotspot_under_threat.pdf (accessed on 19 May 2026).
25. Aurelle, D.; Thomas, S.; Albert, C.; Bally, M.; Bondeau, A.; Boudouresque, C.; Cahill, A.E.; Carlotti, F.; Chenuil, A.; Cramer, W.; et al. Biodiversity, Climate Change, and Adaptation in the Mediterranean. *Ecosphere* **2022**, *13*, e3915. [CrossRef]
26. Vogel, J.; Paton, E.; Aich, V. Seasonal Ecosystem Vulnerability to Climatic Anomalies in the Mediterranean. *Biogeosciences* **2021**, *18*, 5903–5927. [CrossRef]
27. Peñuelas, J.; Sardans, J.; Filella, I.; Estiarte, M.; Llusià, J.; Ogaya, R.; Carnicer, J.; Bartrons, M.; Rivas-Ubach, A.; Grau, O.; et al. Impacts of Global Change on Mediterranean Forests and Their Services. *Forests* **2017**, *8*, 463. [CrossRef]
28. García-Ruiz, J.M.; Arnáez, J.; Lasanta, T.; Nadal-Romero, E.; López-Moreno, J.I. *Mountain Environments: Changes and Impacts*; Springer Nature: Cham, Switzerland, 2024. [CrossRef]
29. Reed, B.C.; Schwartz, M.D.; Xiao, X. Remote Sensing Phenology. In *Phenology of Ecosystem Processes*; Springer: New York, NY, USA, 2009; pp. 231–246. [CrossRef]
30. Caparros-Santiago, J.A.; Rodríguez-Galiano, V.; Dash, J. Land Surface Phenology as Indicator of Global Terrestrial Ecosystem Dynamics: A Systematic Review. *ISPRS J. Photogramm. Remote Sens.* **2021**, *171*, 330–347. [CrossRef]
31. Jones, H.G.; Vaughan, R.A. *Remote Sensing of Vegetation: Principles, Techniques, and Applications*; OUP Oxford: New York, UK, 2010.
32. Zhou, L.; Zhou, W.; Chen, J.; Xu, X.; Wang, Y.; Zhuang, J.; Chi, Y. Land Surface Phenology Detections from Multi-Source Remote Sensing Indices Capturing Canopy Photosynthesis Phenology across Major Land Cover Types in the Northern Hemisphere. *Ecol. Indic.* **2022**, *135*, 108579. [CrossRef]
33. Gutiérrez-Hernández, O.; García, L.V. Robust Trend Analysis in Environmental Remote Sensing: A Case Study of Cork Oak Forest Decline. *Remote Sens.* **2024**, *16*, 3886. [CrossRef]
34. Yue, S.; Wang, C.Y. Applicability of Prewhitening to Eliminate the Influence of Serial Correlation on the Mann-Kendall Test. *Water Resour. Res.* **2002**, *38*, 4-1–4-7. [CrossRef]
35. Gutiérrez-Hernández, O.; García, L.V. Trends in Vegetation Seasonality in the Iberian Peninsula: Spatiotemporal Analysis Using AVHRR-NDVI Data (1982–2023). *Sustainability* **2024**, *16*, 9389. [CrossRef]
36. Gutiérrez-Hernández, O.; García, L.V. The Ghost of Selective Inference in Spatiotemporal Trend Analysis. *Sci. Total Environ.* **2025**, *958*, 177832. [CrossRef] [PubMed]
37. Heumann, B.W. The Multiple Comparison Problem in Empirical Remote Sensing. *Photogramm. Eng. Remote Sens.* **2015**, *81*, 921–926. [CrossRef]
38. Clements, N.; Sarkar, S.K.; Zhao, Z.; Kim, D.-Y. Applying Multiple Testing Procedures to Detect Change in East African Vegetation. *Ann. Appl. Stat.* **2014**, *8*, 286–308. [CrossRef]
39. Gutiérrez-Hernández, O.; García, L.V. Multiple Testing in Remote Sensing: Addressing the Elephant in the Room. 2024. Available online: https://papers.ssrn.com/sol3/papers.cfm?abstract_id=4891512 (accessed on 19 May 2026). [CrossRef]
40. Ulbrich, U.; May, W.; Li, L.; Lionello, P.; Pinto, J.G.; Somot, S. *The Mediterranean Climate Change Under Global Warming*; Elsevier: Amsterdam, The Netherlands, 2006. [CrossRef]
41. Underwood, E.C.; Viers, J.H.; Klausmeyer, K.R.; Cox, R.L.; Shaw, M.R. Threats and Biodiversity in the Mediterranean Biome. *Divers. Distrib.* **2009**, *15*, 188–197. [CrossRef]
42. Ben-Said, M. Upward Shifts of Species Range in Mediterranean High-Mountain Forests Under Current Climate Change: A Review. *Biol. Environ. Proc. R. Ir. Acad.* **2022**, *122B*, 39–52. [CrossRef]
43. Peñuelas, J.; Rutishauser, T.; Filella, I. Phenology Feedbacks on Climate Change. *Science (1979)* **2009**, *324*, 887–888. [CrossRef] [PubMed]
44. Gutiérrez-Hernández, O.; Cámara-Artigas, R.; García, L.V. Regeneration Dynamics of the Baetic Spanish Fir Forests. Inter-Annual and Seasonal Trends Analysis of NDVI. *Pirin. Rev. Ecol. Montaña* **2018**, *173*, e035. [CrossRef]
45. Kottek, M.; Grieser, J.; Beck, C.; Rudolf, B.; Rubel, F. World Map of Köppen−Geiger Climate Classification. *Meteorol. Z.* **2006**, *15*, 259–263. [CrossRef] [PubMed]

46. Navarro-Cerrillo, R.M.; Manzanedo, R.D.; Rodríguez-Vallejo, C.; Gazol, A.; Palacios-Rodríguez, G.; Camarero, J.J. Competition Modulates the Response of Growth to Climate in Pure and Mixed Abies Pinsapo Subsp. Maroccana Forests in Northern Morocco. *For. Ecol. Manag.* **2020**, *459*, 117847. [CrossRef]
47. Gutiérrez-Hernández, O. A Short Note on the Distribution and Tree Cover of the Moroccan Fir (*Abies marocana* Trab.) in Talassemtane National Park (Western Rif). *Pirineos*, accepted for publication. 2026. [CrossRef] [PubMed]
48. Gutiérrez-Hernández, O. Mapping the Distribution of *Abies marocana*: Geospatial Reference Data for Biogeographical Research and Conservation. In *Proceedings of the 2025 EUROGEO Annual Meeting and Conference*; EUROGEO: Skopje, North Macedonia, 2025. [CrossRef]
49. Chergui, B.; Fahd, S.; Santos, X.; Pausas, J.G. Moroccan Cannabis Farms Threaten Biodiversity. *Science (1979)* **2024**, *385*, 941. [CrossRef]
50. Castro, I.; Stan, A.B.; Taïqui, L.; Schiefer, E.; Ghallab, A.; Derak, M.; Fulé, P.Z. Detecting Fire-Caused Forest Loss in a Moroccan Protected Area. *Fire* **2022**, *5*, 51. [CrossRef]
51. Huete, A.; Didan, K.; Miura, T.; Rodríguez, E.P.; Gao, X.; Ferreira, L.G. Overview of the Radiometric and Biophysical Performance of the MODIS Vegetation Indices. *Remote Sens. Environ.* **2002**, *83*, 195–213. [CrossRef]
52. Rouse, J.; Haas, R.; Schell, J. *Monitoring the Vernal Advancement and Retrogradation (Greenwave Effect) of Natural Vegetation*; Texas A & M University: College Station, TX, USA, 1974; pp. 1–8. Available online: https://ntrs.nasa.gov/citations/19740022555 (accessed on 19 May 2026).
53. Huete, A.R.; Didan, K.; Shimabukuro, Y.E.; Ratana, P.; Saleska, S.R.; Hutyra, L.R.; Yang, W.; Nemani, R.R.; Myneni, R. Amazon Rainforests Green-up with Sunlight in Dry Season. *Geophys. Res. Lett.* **2006**, *33*. [CrossRef]
54. Kaufman, Y.J.; Tanre, D. Atmospherically Resistant Vegetation Index (ARVI) for EOS-MODIS. *IEEE Trans. Geosci. Remote Sens.* **1992**, *30*, 261–270. [CrossRef]
55. Didan, K. MODIS/Terra Vegetation Indices 16-Day L3 Global 250m SIN Grid V061 [Data Set]. 2021. Available online: https://www.earthdata.nasa.gov/data/catalog/lpcloud-mod13q1-061 (accessed on 23 February 2026).
56. Roerink, G.J.; Menenti, M.; Verhoef, W. Reconstructing Cloudfree NDVI Composites Using Fourier Analysis of Time Series. *Int. J. Remote Sens.* **2000**, *21*, 1911–1917. [CrossRef]
57. Eastman, J. *Earth Trends Modeler*; Version 20 (liberaGIS); Clark Center for Geospatial Analytics (ClarkCGA), Clark University: Worcester, MA, USA, 2025. Available online: https://www.clarku.edu/geospatial-analytics/ (accessed on 25 May 2026).
58. Gutiérrez-Hernández, O. The Baetic-Rifan Firs (Abies Pinsapo and *Abies marocana*): Geospatial Reference Data for Comparative Analysis and Conservation of the Westernmost Circum-Mediterranean Firs. In *Proceedings of the 7th International Congress on Biodiversity and Nature Conservation (Conserbio 2025)*; Conserbio: Seville, Spain, 2025. [CrossRef]
59. Gutiérrez-Hernández, O. Distribution and Tree Cover of the Moroccan Fir (*Abies marocana* Trab.) in Talassemtane National Park (Western Rif, Northern Morocco) [Dataset]. 2025. Available online: https://riuma.uma.es/entities/publication/f193eb82-68bc-4354-8269-b2fb674ef4e0 (accessed on 25 May 2026). [CrossRef]
60. Hijmans, R.J. *terra: Spatial Data Analysis*, R Package Version 1.9-27; 2025. Available online: https://CRAN.R-project.org/package=terra (accessed on 25 May 2026).
61. Eastman, J.R.; Clark Labs. *TerrSet: Geospatial Monitoring and Modeling Software*; Version 20; Clark University: Worcester, MA, USA, 2024.
62. Eastman, J.R.; Sangermano, F.; Ghimire, B.; Zhu, H.; Chen, H.; Neeti, N.; Cai, Y.; Machado, E.A.; Crema, S.C. Seasonal Trend Analysis of Image Time Series. *Int. J. Remote Sens.* **2009**, *30*, 2721–2726. [CrossRef]
63. Eastman, J.R.; Sangermano, F.; Machado, E.A.; Rogan, J.; Anyamba, A. Global Trends in Seasonality of Normalized Difference Vegetation Index (NDVI), 1982–2011. *Remote Sens.* **2013**, *5*, 4799–4818. [CrossRef]
64. Wang, X.L.; Swail, V.R. Changes of Extreme Wave Heights in Northern Hemisphere Oceans and Related Atmospheric Circulation Regimes. *J. Clim.* **2001**, *14*, 2204–2221. [CrossRef]
65. Durbin, J.; Watson, G.S. Testing for Serial Correlation in Least Squares Regression: I. *Biometrika* **1950**, *37*, 409–428. [CrossRef]
66. Durbin, J.; Watson, G.S. Testing for Serial Correlation in Least Squares Regression: II. *Biometrika* **1951**, *38*, 159–178. [CrossRef]
67. Neeti, N.; Eastman, J.R. A Contextual Mann-Kendall Approach for the Assessment of Trend Significance in Image Time Series. *Trans. GIS* **2011**, *15*, 599–611. [CrossRef]
68. Benjamini, Y. Discovering the False Discovery Rate. *J. R. Stat. Soc. Ser. B Stat. Methodol.* **2010**, *72*, 405–416. [CrossRef]
69. Benjamini, Y.; Hochberg, Y. Controlling the False Discovery Rate: A Practical and Powerful Approach to Multiple Testing. *J. R. Stat. Soc. Ser. B (Methodol.)* **1995**, *57*, 289–300. [CrossRef]
70. Gutiérrez-Hernández, O.; García, L.V. False Discovery Rate Estimation and Control in Remote Sensing: Reliable Statistical Significance in Spatially Dependent Gridded Data. *Remote Sens. Lett.* **2025**, *16*, 537–548. [CrossRef]
71. Eklundh, L.; Jönsson, P. TIMESAT: A Software Package for Time-Series Processing and Assessment of Vegetation Dynamics. In *Remote Sensing Time Series*; Springer: Berlin/Heidelberg, Germany, 2015; pp. 141–158. [CrossRef]

72. Zhang, X.; Friedl, M.A.; Schaaf, C.B.; Strahler, A.H.; Hodges, J.C.F.; Gao, F.; Reed, B.C.; Huete, A. Monitoring Vegetation Phenology Using MODIS. *Remote Sens. Environ.* **2003**, *84*, 471–475. [CrossRef]
73. Zeng, L.; Wardlow, B.D.; Xiang, D.; Hu, S.; Li, D. A Review of Vegetation Phenological Metrics Extraction Using Time-Series, Multispectral Satellite Data. *Remote Sens. Environ.* **2020**, *237*, 111511. [CrossRef]
74. Reed, B.C. Trend Analysis of Time-Series Phenology of North America Derived from Satellite Data. *GIsci. Remote Sens.* **2006**, *43*, 24–38. [CrossRef]
75. Gonsamo, A.; Chen, J.M.; Ooi, Y.W. Peak Season Plant Activity Shift towards Spring Is Reflected by Increasing Carbon Uptake by Extratropical Ecosystems. *Glob. Change Biol.* **2018**, *24*, 2117–2128. [CrossRef]
76. Myneni, R.B.; Keeling, C.D.; Tucker, C.J.; Asrar, G.; Nemani, R.R. Increased Plant Growth in the Northern High Latitudes from 1981 to 1991. *Nature* **1997**, *386*, 698–702. [CrossRef]
77. Peñuelas, J.; Filella, I.; Comas, P. Changed Plant and Animal Life Cycles from 1952 to 2000 in the Mediterranean Region. *Glob. Change Biol.* **2002**, *8*, 531–544. [CrossRef]
78. Piao, S.; Friedlingstein, P.; Ciais, P.; de Noblet-Ducoudré, N.; Labat, D.; Zaehle, S. Changes in Climate and Land Use Have a Larger Direct Impact than Rising CO_2 on Global River Runoff Trends. *Proc. Natl. Acad. Sci. USA* **2007**, *104*, 15242–15247. [CrossRef] [PubMed]
79. Richardson, A.D.; Keenan, T.F.; Migliavacca, M.; Ryu, Y.; Sonnentag, O.; Toomey, M. Climate Change, Phenology, and Phenological Control of Vegetation Feedbacks to the Climate System. *Agric. For. Meteorol.* **2013**, *169*, 156–173. [CrossRef]
80. Gao, M.; Piao, S.; Chen, A.; Yang, H.; Liu, Q.; Fu, Y.H.; Janssens, I.A. Divergent Changes in the Elevational Gradient of Vegetation Activities over the Last 30 Years. *Nat. Commun.* **2019**, *10*, 2970. [CrossRef] [PubMed]
81. Guyon, D.; Guillot, M.; Vitasse, Y.; Cardot, H.; Hagolle, O.; Delzon, S.; Wigneron, J.-P. Monitoring Elevation Variations in Leaf Phenology of Deciduous Broadleaf Forests from SPOT/VEGETATION Time-Series. *Remote Sens. Environ.* **2011**, *115*, 615–627. [CrossRef]
82. Ma, S.; Pitman, A.J.; Lorenz, R.; Kala, J.; Srbinovsky, J. Earlier Green-up Amplifies Spring Warming over Europe. *Geophys. Res. Lett.* **2016**, *46*, 582–589. [CrossRef]
83. Buitenwerf, R.; Rose, L.; Higgins, S.I. Three Decades of Multi-Dimensional Change in Global Leaf Phenology. *Nat. Clim. Change* **2015**, *5*, 364–368. [CrossRef]
84. Jönsson, P.; Eklundh, L. Seasonality Extraction by Function Fitting to Time-Series of Satellite Sensor Data. *IEEE Trans. Geosci. Remote Sens.* **2002**, *40*, 1824–1832. [CrossRef]
85. White, M.A.; Thornton, P.E.; Running, S.W. A Continental Phenology Model for Monitoring Vegetation Responses to Interannual Climatic Variability. *Glob. Biogeochem. Cycles* **1997**, *11*, 217–234. [CrossRef]
86. Jönsson, P.; Eklundh, L. TIMESAT—A Program for Analyzing Time-Series of Satellite Sensor Data. *Comput. Geosci.* **2004**, *30*, 833–845. [CrossRef]
87. Körner, C. *Alpine Treelines*; Springer: Basel, Switzerland, 2012.
88. Mountain Research Initiative EDW Working Group. Elevation-Dependent Warming in Mountain Regions of the World. *Nat. Clim. Change* **2015**, *5*, 424–430. [CrossRef]
89. Nemani, R.R.; Keeling, C.D.; Hashimoto, H.; Jolly, W.M.; Piper, S.C.; Tucker, C.J.; Myneni, R.B.; Running, S.W. Climate-Driven Increases in Global Terrestrial Net Primary Production from 1982 to 1999. *Science (1979)* **2003**, *300*, 1560–1563. [CrossRef] [PubMed]
90. Gutiérrez-Hernández, O. Tendencias Recientes Del NDVI En Andalucía: Los Límites Del Reverdecimiento. *Boletín De La Asoc. De Geógrafos Españoles* **2022**, *94*, 1–36. [CrossRef]
91. Vicente-Serrano, S.M.; Domínguez-Castro, F.; Murphy, C.; Peña-Angulo, D.; Tomas-Burguera, M.; Noguera, I.; López-Moreno, J.I.; Juez, C.; Grainger, S.; Eklundh, L.; et al. Increased Vegetation in Mountainous Headwaters Amplifies Water Stress During Dry Periods. *Geophys. Res. Lett.* **2021**, *48*, e2021GL094672. [CrossRef]
92. Gutiérrez-Hernández, O.; García, L.V. Uncovering True Significant Trends in Global Greening. *Remote Sens. Appl.* **2025**, *37*, 101377. [CrossRef]
93. Westerling, A.L.; Hidalgo, H.G.; Cayan, D.R.; Swetnam, T.W. Warming and Earlier Spring Increase Western U.S. Forest Wildfire Activity. *Science (1979)* **2006**, *313*, 940–943. [CrossRef] [PubMed]
94. Gutiérrez-Hernández, O.; García, L.V. Implementing the Linear Adaptive False Discovery Rate Procedure for Spatiotemporal Trend Testing. *Mathematics* **2025**, *13*, 3630. [CrossRef]
95. Glenn, E.P.; Huete, A.R.; Nagler, P.L.; Nelson, S.G. Relationship Between Remotely-Sensed Vegetation Indices, Canopy Attributes and Plant Physiological Processes: What Vegetation Indices Can and Cannot Tell Us About the Landscape. *Sensors* **2008**, *8*, 2136–2160. [CrossRef] [PubMed]
96. Huemmrich, K.F.; Vargas Zesati, S.; Campbell, P.; Tweedie, C. Canopy Reflectance Models Illustrate Varying NDVI Responses to Change in High Latitude Ecosystems. *Ecol. Appl.* **2021**, *31*, e02435. [CrossRef] [PubMed]
97. Wang, H.; Muller, J.D.; Tatarinov, F.; Yakir, D.; Rotenberg, E. Disentangling Soil, Shade, and Tree Canopy Contributions to Mixed Satellite Vegetation Indices in a Sparse Dry Forest. *Remote Sens.* **2022**, *14*, 3681. [CrossRef]

98. Ma, X.; Zhu, X.; Xie, Q.; Jin, J.; Zhou, Y.; Luo, Y.; Liu, Y.; Tian, J.; Zhao, Y. Monitoring Nature's Calendar from Space: Emerging Topics in Land Surface Phenology and Associated Opportunities for Science Applications. *Glob. Change Biol.* **2022**, *28*, 7186–7204. [CrossRef] [PubMed]
99. Lu, X.; Liu, Z.; Zhou, Y.; Liu, Y.; An, S.; Tang, J. Comparison of Phenology Estimated from Reflectance-Based Indices and Solar-Induced Chlorophyll Fluorescence (SIF) Observations in a Temperate Forest Using GPP-Based Phenology as the Standard. *Remote Sens.* **2018**, *10*, 932. [CrossRef]
100. Li, M.; Cao, S.; Zhu, Z.; Wang, Z.; Myneni, R.B.; Piao, S. Spatiotemporally Consistent Global Dataset of the GIMMS Normalized Difference Vegetation Index (PKU GIMMS NDVI) from 1982 to 2022. *Earth Syst. Sci. Data* **2023**, *15*, 4181–4203. [CrossRef]
101. Dronova, I.; Taddeo, S. Remote Sensing of Phenology: Towards the Comprehensive Indicators of Plant Community Dynamics from Species to Regional Scales. *J. Ecol.* **2022**, *110*, 1460–1484. [CrossRef]
102. Wulder, M.A.; Roy, D.P.; Radeloff, V.C.; Loveland, T.R.; Anderson, M.C.; Johnson, D.M.; Healey, S.; Zhu, Z.; Scambos, T.A.; Pahlevan, N.; et al. Fifty Years of Landsat Science and Impacts. *Remote Sens. Environ.* **2022**, *280*, 113195. [CrossRef]
103. Girardello, M.; Checcherini, G.; Duveiller, G.; Migliavacca, M.; Cescatti, A. Patterns and Trends in the Spatial Heterogeneity of Land Surface Phenology of Global Forests. *Environ. Res. Commun.* **2024**, *6*, 041004. [CrossRef]
104. Chen, R.; Yin, G.; Liu, G.; Li, J.; Verger, A. Evaluation and Normalization of Topographic Effects on Vegetation Indices. *Remote Sens.* **2020**, *12*, 2290. [CrossRef]
105. Peñuelas, J.; Sardans, J. Global Change and Forest Disturbances in the Mediterranean Basin: Breakthroughs, Knowledge Gaps, and Recommendations. *Forests* **2021**, *12*, 603. [CrossRef]

Disclaimer/Publisher's Note: The statements, opinions and data contained in all publications are solely those of the individual author(s) and contributor(s) and not of MDPI and/or the editor(s). MDPI and/or the editor(s) disclaim responsibility for any injury to people or property resulting from any ideas, methods, instructions or products referred to in the content.